2016

Left hemisphere structural connectivity abnormality in pediatric hydrocephalus patients following surgery

Weihong Yuan
University of Cincinnati

Artur Meller
Cincinnati Children's Hospital Medical Center

Joshua S. Shimony
Washington University School of Medicine in St. Louis

Tiffany Nash
Cincinnati Children's Hospital Medical Center

Blaise V. Jones
University of Cincinnati

See next page for additional authors

NeuroImage: Clinical 12 (2016) 631–639

Contents lists available at ScienceDirect

NeuroImage: Clinical

journal homepage: www.elsevier.com/locate/ynicl

Left hemisphere structural connectivity abnormality in pediatric hydrocephalus patients following surgery

Weihong Yuan[a,e,*], Artur Meller[a], Joshua S. Shimony[f], Tiffany Nash[a], Blaise V. Jones[a,e], Scott K. Holland[a,e], Mekibib Altaye[c,e], Holly Barnard[b,e], Jannel Phillips[b,e], Stephanie Powell[g,h], Robert C. McKinstry[f], David D. Limbrick[i], Akila Rajagopal[a], Francesco T. Mangano[d,e]

[a]Department of Radiology, Cincinnati Children's Hospital Medical Center, Cincinnati, OH, United States
[b]Division of Developmental and Behavioral Pediatrics – Psychology, Cincinnati Children's Hospital Medical Center, Cincinnati, OH, United States
[c]Division of Biostatistics and Epidemiology, Cincinnati Children's Hospital Medical Center, Cincinnati, OH, United States
[d]Division of Pediatric Neurosurgery, Cincinnati Children's Hospital Medical Center, Cincinnati, OH, United States
[e]University of Cincinnati College of Medicine, Cincinnati, OH, United States
[f]Mallinckrodt Institute of Radiology, Washington University School of Medicine, Saint Louis, MO, United States
[g]Department of Neurology, Washington University School of Medicine, Saint Louis, MO, United States
[h]Department of Psychology, St. Louis Children's Hospital, St. Louis, MO, United States
[i]Department of Neurological Surgery, Washington University School of Medicine, Saint Louis, MO, United States

ARTICLE INFO

Article history:
Received 1 June 2016
Received in revised form 19 August 2016
Accepted 2 September 2016
Available online 04 September 2016

Keywords:
Diffusion tensor imaging
Graph theoretical analysis
Left hemisphere
Pediatric hydrocephalus
Small-worldness

ABSTRACT

Neuroimaging research in surgically treated pediatric hydrocephalus patients remains challenging due to the artifact caused by programmable shunt. Our previous study has demonstrated significant alterations in the whole brain white matter structural connectivity based on diffusion tensor imaging (DTI) and graph theoretical analysis in children with hydrocephalus prior to surgery or in surgically treated children without programmable shunts. This study seeks to investigate the impact of brain injury on the topological features in the left hemisphere, contratelateral to the shunt placement, which will avoid the influence of shunt artifacts and makes further group comparisons feasible for children with programmable shunt valves. Three groups of children (34 in the control group, 12 in the 3-month post-surgery group, and 24 in the 12-month post-surgery group, age between 1 and 18 years) were included in the study. The structural connectivity data processing and analysis were performed based on DTI and graph theoretical analysis. Specific procedures were revised to include only left brain imaging data in normalization, parcellation, and fiber counting from DTI tractography. Our results showed that, when compared to controls, children with hydrocephalus in both the 3-month and 12-month post-surgery groups had significantly lower normalized clustering coefficient, lower small-worldness, and higher global efficiency (all $p < 0.05$, corrected). At a regional level, both patient groups showed significant alteration in one or more regional connectivity measures in a series of brain regions in the left hemisphere (8 and 10 regions in the 3-month post-surgery and the 12-month post-surgery group, respectively, all $p < 0.05$, corrected). No significant correlation was found between any of the global or regional measures and the contemporaneous neuropsychological outcomes [the General Adaptive Composite (GAC) from the Adaptive Behavior Assessment System, Second Edition (ABAS-II)]. However, one global network measure (global efficiency) and two regional network measures in the insula (local efficiency and between centrality) tested at 3-month post-surgery were found to correlate with GAC score tested at 12-month post-surgery with statistical significance (all $p < 0.05$, corrected). Our data showed that the structural connectivity analysis based on DTI and graph theory was sensitive in detecting both global and regional network abnormality when the analysis was conducted in the left hemisphere only. This approach provides a new avenue enabling the application of advanced neuroimaging analysis methods in quantifying brain damage in children with hydrocephalus surgically treated with programmable shunts.

Abbreviations: DTI, diffusion tensor imaging; ROI, region of interest.

* Corresponding author at: Pediatric Neuroimaging Research Consortium, Department of Radiology, Cincinnati Children's Hospital, 3333 Burnet Avenue, ML 5033, Cincinnati, OH 45229, United States.
E-mail address: Weihong.Yuan@cchmc.org (W. Yuan).

http://dx.doi.org/10.1016/j.nicl.2016.09.003

1. Introduction

Hydrocephalus is a neurological disorder that affects 1 out of 2000 live births and represents roughly 1/3 of all congenital central nervous system anomalies (Wiswell et al., 1990). Pediatric hydrocephalus is a commonly treatable but incurable condition with variable long-term prognosis and outcome (Hirsch, 1992). White matter (WM) structures in patients with hydrocephalus have been found to be vulnerable as the result of ventriculomegaly and elevated intracranial pressure, leading to subsequent behavioral and neuropsychological deficits (Mataro et al., 2001). Using diffusion tensor imaging (DTI), microstructural damage has been identified in a wide range of WM regions in this patient population at both pre- and post-surgical stages. However, most of these studies were based on the extraction of DTI values from a pre-defined list of regions of interest, usually including several important but limited number of major WM structures such as the corpus callosum, anterior and posterior limb of internal capsule, corticospinal tract, and superior and inferior longitudinal fasciculus (Assaf et al., 2006; Hasan et al., 2008; Yuan et al., 2009, Air et al., 2010; Scheel et al., 2012; Rajagopal et al., 2013; Jang et al., 2013; Yuan et al., 2013; Ben-Sira et al., 2015; Kulkarni et al., 2015; Mangano et al., 2016).

In the present study, WM structural integrity in pediatric hydrocephalus was studied after surgical treatment based on graph theoretical analysis and DTI tractography. This approach has recently emerged as a promising tool that provides information on the integrity of the structural connectivity of brain networks, at both global and regional levels (Rubinov and Sporns, 2010). The application of this approach has generated many new perspectives in the study of neurological disorders, including a recent study of pediatric hydrocephalus (Caeyenberghs et al., 2012; Liu et al., 2014; Pereira et al., 2015; Sun et al., 2016; Yuan et al., 2015). However, there is a unique difficulty in using this technique to study hydrocephalus in patients after their surgical treatment as many patients with hydrocephalus are treated by a shunting procedure that incorporates a programmable valve. The post-surgery MRI scans often contain artifacts from the metallic components of the programmable valves, making the graph analysis based on whole brain WM tractography unworkable.

In order to overcome this obstacle, we investigated the application of structural connectivity analysis in children with hydrocephalus post-surgery based on graph theory and tractography using the left hemisphere only. Except for rare situations when the neuroanatomy or other medical or surgical considerations contradict it, ventricular shunts are usually inserted through a burhole in the right frontal region. Consequently, the left hemisphere is usually not involved in the surgery and remains artifact free in MRI. We seek to investigate the impact of brain injury on the topological features in the left hemisphere network, which will avoid the influence of shunt artifacts and make image normalization and further group comparisons feasible for children with programmable shunts. In our previous study, significant alterations in structural connectivity indices were seen in children with hydrocephalus prior to surgery and in children post-operatively without imaging artifacts from programmable valves. Therefore, the working hypotheses of the present study are: (1) the post-surgical WM structural connectivity of the left hemisphere, when assessed alone, is affected in hydrocephalus patients as reflected in the aberrant topological features at both the global and regional level; (2) network measures of the left hemisphere are significantly correlated with neurodevelopmental outcome measures in children with hydrocephalus post-surgery.

2. Materials and methods

2.1. Participants

The data in the present study were selected from a prospective neuroimaging project of children treated for hydrocephalus (Buckley et al., 2012; Yuan et al., 2013; Rajagopal et al., 2013; Akbari et al., 2015; Ragan et al., 2015; Yuan et al., 2015; Mangano et al., 2016). At the time of data analysis, 64 control children and 56 children with hydrocephalus were identified as eligible candidates for the present study. After initial testing of data processing and analysis, it was decided that datasets from children younger than 11 months needed to be excluded because the poor image contrast in very young children made it difficult to generate consistent results during image normalization. In addition, five participants (3 controls and two hydrocephalus patients) were initially eligible for the study but were later excluded due to excessive head motion ($n = 4$) or image distortion ($n = 1$). Combining these factors, three groups of children were included in the final analysis. Group 1, controls, $n = 34$, age range: 12.1–197.8 months, median age 51.2 months; Group 2, children with hydrocephalus at 3-month post-surgery, $n = 12$, age range: 14.3–199.4 months, median age 35.5 months; and Group 3: children with hydrocephalus at 12 month post-surgery, $n = 24$, age range: 11.2–207.2 months, median age 22.7 months. No statistically significant difference was found in age between the control group and either of the two patient groups ($p > 0.2$). The 34 children in the control group came from two sources. (1) 19 of the 34 children in the control group were recruited from pediatric patients referred to radiology for clinical MRI for non-specific symptoms not clearly related to a neurological disorder (e.g. headaches). These children had no clinical or radiographic history of neurological or psychological disorders and there was no evidence of any neurological disorders (e.g., epilepsy) or suggestion of white matter related brain pathology upon review of the patient's medical record at 3 months after the MRI scan. This 3-month follow-up chart analysis was completed to ensure that we did not include anyone who may have developed a central nervous system pathology after the MRI scan. (2) 15 of the 34 children from the control group were recruited from healthy population. The MRI scans for these healthy normal controls were acquired under research protocol on the same scanners but without sedation. Between the two patient groups, there was an overlap of six children who had imaging data at both 3-month and 12-month post-surgery. In these 6 children with hydrocephalus, no statistically significant longitudinal difference was found in any of the network measures or behavioral outcome measure. Therefore, no specific discussion was made in this subset of participants.

All the participants were recruited from two children's hospitals: Cincinnati Children's Hospital (CCHMC) and St. Louis Children's Hospital (SLCH). The study was approved by the Institutional Review Board at both CCHMC and SLCH (Washington University). Families of participants gave written informed consent when enrolled into the study, and children older than 11 years of age provided written assent.

2.2. MRI/DTI data acquisition

DTI data were acquired with a single-shot, echo-planar imaging sequence on three 1.5 Tesla scanners, including two scanners at CCHMC (GE Signa, GE Healthcare, Milwaukee, Wisconsin) and one scanner at SLCH (Siemens Avanto, Erlangen, Germany). The sequence specifications were: 15 non-collinear diffusion encoding directions; b = 0, 1000 s/mm^2; TR/TE = 9400/93.2 ms; field of view = 240 mm × 240 mm; matrix = 96 × 96; in-plan resolution = 2.5 mm × 2.5 mm; slice thickness = 2.5 mm; ASSET (on GE scanner) or IPAT (on Siemens scanner) factor = 2; number of average = 2. The data in the present study were selected from a larger prospective neuroimaging project of children treated for hydrocephalus. Before the start of the study, we used the fBIRN phantom and traveling human phantom to test MRI protocol and to establish the compatibility of scan results across sites and scanners (two 1.5T GE scanners at CCHMC ad one 1.5T Siemens scanner at SLCH). After the study started, the same process was repeated annually to confirm the compatibility throughout the duration of the study. The protocol also included the collection of QA data using ACR phantoms shortly after the subject's scan (within a week) to assure the stability of scanner performance and to detect potential system performance change relative to established baseline. As reported elsewhere (Yuan et al., 2011), the scanners showed high compatibility

during initial setup and also during the entire study period. As shown in a previous report, when tested as a potential source of variability, the scanner was not found to be a significant factor in the statistical analysis (Yuan et al., 2013). More details about the initial site/scanner compatibility, its annual assessment, as well as the routine quality assurance procedures have been reported in previous work. (Yuan et al., 2011; Rajagopal et al., 2013; Yuan et al., 2013; Yuan et al., 2015; Mangano et al., 2016).

2.3. DTI data preprocessing and brain parcellation

Head motion and eddy current artifacts in the DTI data were corrected using the Automated Image Registration method (Woods et al., 1998). The B-matrix was rotated according to the subject motion correction (Leemans and Jones, 2009). The DTI metrics maps were calculated with standard technique (Basser and Pierpaoli, 1998). Using MRI Studio (Jiang et al., 2006), the right hemisphere was manually masked to leave only the left hemisphere for subsequent data analysis (Fig. 1). Large deformation diffeomorphic metric mapping, a non-linear transformation, was used to normalize the images to MNI space to register with the JHU-DTI-WMPM II atlas (Oishi et al., 2008; Oishi et al., 2009; Djamanakova et al., 2013). DTI maps with multiple contrasts (FA and b0, all with only left hemisphere) were used to provide complementary contrast in the normalization. Mask of ventricles in b0 maps were used for hydrocephalus patients to improve registration. The parcellation of gray and white matter from the atlas were then inversely transformed back to the subject space and used for parcellating the brain into 65 brain regions in the left hemisphere. From these 65 regions, the 31 cortical and subcortical regions in the left hemisphere were retained for the later fiber counting procedure. The name and abbreviations for these 31 regions are identical to previously reported ones (see Table 2 in Yuan et al., 2015).

In subjects' native space, left brain WM fiber tracking was conducted using Diffusion Toolkit/TrackVis (Wang et al., 2007; http://trackvis.org/dtk/). Tractography was performed using a deterministic tracking algorithm (FACT: fiber assignment by continuous tracking). An angular threshold of 70° was applied for the tractography.

2.4. Graph theoretical analysis

Graph theoretical analysis was performed on the above described 31×31 matrix for the left hemisphere using the Brain Connectivity Toolbox (Rubinov and Sporns, 2010). Five standard global connectivity measures (small-worldness (σ), normalized clustering coefficient (γ), normalized characteristic path length (λ), global efficiency (Eglob), and modularity(MOD)) and four standard regional connectivity measures (nodal degree, nodal clustering coefficient (CC), nodal local efficiency (Eloc), and between-ness centrality (BC)) were calculated and compared. Standard methods were used in the present study, and all the formulas for calculating the network measures can be found in the literature (Rubinov and Sporns, 2010). Only brief descriptions are provided as follows.

In a network of nodes and edges that connect nodes, the clustering coefficient (C) is a measure of network segregation. It is calculated as the mean of nodal clustering coefficients across the network, with the nodal clustering coefficient defined as the ratio between the number of edges among the neighbors of the node and the maximum possible number of edges among these neighbors. The characteristic path length (Lp) is a global property that measures the level of integration of the network. It is calculated as the mean of the shortest path lengths between any two nodes in the network, with the shortest path length defined as the smallest possible number of edges that need to be traversed between two nodes. The small-worldness (σ) is a global network measure that quantifies the balance between segregation and integration in the network. It is calculated as the ratio between the normalized clustering coefficient (γ) and the normalized characteristic path length (λ). In order to normalize network measures, we generated a random network rewired with the same degree distribution as the actual brain network, repeated this simulation 1000 times, and used the mean values from the simulated random network as the denominator of the normalized clustering coefficient ($\gamma = C/Crand$) and the normalized characteristic path length ($\lambda = Lp/Lprand$), respectively. Therefore, the small-worldness is calculated as follows: $\sigma = \gamma/\lambda = (C/Crand)\ /\ (Lp/Lprand)$. Typically, a network is considered to have small world feature if it satisfies the following conditions: $\gamma \gg 1$, $\lambda \approx 1$, and $\sigma \gg 1$ (Watts and Strogatz, 1998; Achard et al., 2006; Humphries et al., 2006). Global efficiency (Eglob) is also a global property that quantifies the network's capacity for integration. It is defined as the harmonic inverse average of shortest path length; thus, it is a reflection of how efficiently information can be transferred in the network. Modularity (MOD) quantifies the degree of network partitioning into modules (smaller networks) where nodes within the same module are densely inter-connected but only have sparse connections with nodes from other modules.

Among the four regional network measures investigated in the present study, the nodal degree (Deg) is the number of edges connecting the given node to other nodes. The nodal clustering coefficient (CC) has been defined in the above description for the network clustering coefficient: it is the ratio between the number of edges among the neighbors of the given node and the maximum possible number of connections among these neighbors. The nodal betweeness centrality (BC) is the ratio between the number of shortest path length connecting other nodes that pass through the node of interest and the total number of shortest path length connecting these nodes. The nodal local efficiency

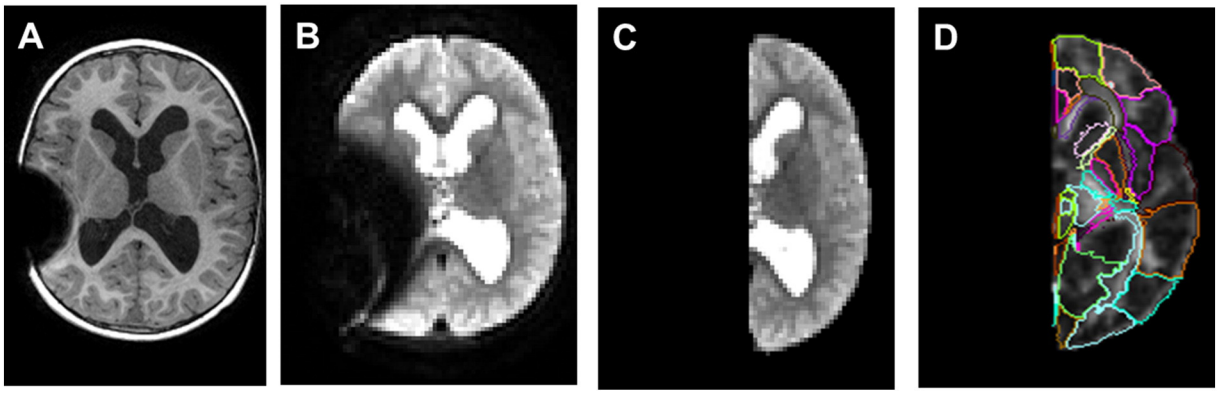

Fig. 1. Example of MRI artifact from programmable shunt valve and the removal of the right hemisphere (along with the artifact) for subsequent data analysis. A. T1-w image with shunt artifact. B. b0 DTI image with shunt artifact; C. b0 DTI image of left hemisphere after the removal of right hemisphere image; D. the results of brain segmentation using let hemisphere alone.

(Eloc) is the inverse of the average of shortest path length in the subgraph defined as the set of nodes that are the neighbors of the node of interest.

2.5. Network density threshold selection

The network density is defined as the ratio between the number of actual edges and the number of maximum possible edges (the full network). In this study, to avoid the potential influence of arbitrarily selected single network density, each network matrix was thresholded over a range of density values from 0.2 to 0.4 at interval of 0.01. In a network of 31 nodes (as used in the present study), the maximum possible number of edges is 465 and the density range of 0.2 to 0.4 represents a range of 93–186 edges. As some network measures in the present study demonstrated age dependence, a linear regression analysis was first applied for each of these network measures and the residual values were used in the subsequent analysis in order to account for age effect. We calculated all the global and regional network measures (using the residual value) at each of the above mentioned 21 density threshold levels and integrated the results for each network index. The calculation of this area under curve (AUC, Fig. 2) generated a summarized scalar that has been used in the field to control for spurious findings as the results of selection of any single density threshold and has been used in detecting brain network topological changes in various patient populations (He et al., 2009; Li et al., 2014; Dennis et al., 2013; Ding et al., 2013).

2.6. Developmental outcomes

The Adaptive Behavior Assessment System, Second Edition (ABAS-II, Harrison and Oakland, 2003) was included in the present study to assess functional outcome. The ABAS-II is a caregiver report form of adaptive skills yielding an overall adaptive score, the General Adaptive Composite (GAC), and three domain scores assessing Conceptual, Social, and Practical skills. It is a norm-referenced standardized measure, with scores derived from comparisons to a normative same of same-age peers. The ABAS-II was administered as part of a larger test battery and the results were reported in our previous work. In the present study, the GAC was used as the primary outcome index. The test was administered by pediatric neuropsychologists or by psychometrists supervised by pediatric neuropsychologists at either the Division of Developmental and Behavioral Pediatrics at CCHMC or the Department of Psychology at SLCH/WashU. During the initial testing of potential confounding factor for neuropsychological outcome, we examined the distribution of GAC testing results plotted against age. No significant correlation was observed between GAC and age, confirming the age normed nature of the ABAS-II testing data collected from the present study. Therefore, age was not included in the eventual analysis of neuropsychological data in association with the network measures.

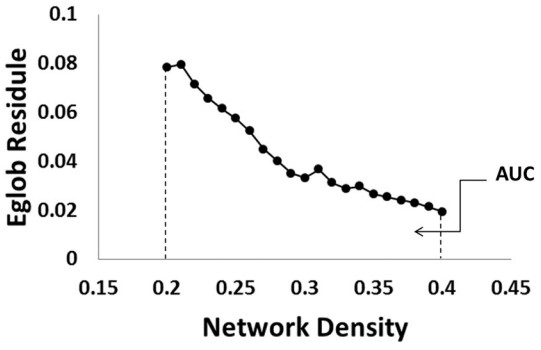

Fig. 2. Example of individual participant's network connectivity index (global efficiency of a child with hydrocephalus at 12-month post-surgery) as a function of network density over the range between 0.2 and 0.4. The residual value of the variable after regressing out the age factor was first calculated at each density threshold. The area under the curve (AUC) was calculated by integrating the residual value of the connectivity index across the range of network density. The AUC of the individual was used in the subsequent group analyses.

2.7. Statistical analysis

Using the integrated AUC based on the residual values after regressing out the age factor and over the range of density 0.2–0.4 with interval of 0.01, group differences in network connectivity variables were tested with two tailed *t*-test at significance level of $p < 0.05$ with multiple comparison correction using the false discovery rate (FDR) method. At the global level, the FDR method was applied for each patient group separately to correct for potential false positive findings in the five global network measures. At the regional level, the FDR correction was also applied for each patient group separately but across all four regional network measures and the 31 network nodes. No correction was performed for the 21 density levels since no multiple comparisons were performed separately over this variable. For those network indices and regions that showed significant group difference between patients and controls, the Pearson correlation analysis was used in the patient groups to quantify the association between structural connectivity measures and contemporaneous neuropsychological outcome measures as well as the association between network measures at 3-months post-surgery and the neuropsychological outcome measures assessed at 12-month post-surgery. Multiple comparison correction was also performed using FDR method in the correlation analysis.

3. Results

3.1. Small-worldness in left hemispheric network

As shown in Fig. 3, the left hemisphere network in all three study groups (the control group and the two hydrocephalus groups) met criteria of small-worldness, i.e., having a $\gamma \gg 1$, $\lambda \approx 1$, and $\sigma \gg 1$ (Watts and Strogatz, 1998; Achard et al., 2006; Humphries et al., 2006), within the network density range (0.2–0.4) selected in the study.

3.2. Abnormal left hemispheric global connectivity measures in children with hydrocephalus (Table 1, all p values FDR corrected)

Compared to the controls, children with hydrocephalus at 3 months post-surgery had significantly lower normalized clustering coefficient ($p = 0.0038$), lower small-worldness (corrected $p = 0.0026$), and higher global efficiency (corrected $p < 0.0001$). Children with hydrocephalus at 12 months post-surgery also had significantly lower normalized clustering coefficient (corrected $p = 0.0086$), lower small-worldness (corrected $p = 0.0113$), and higher global efficiency (corrected $p < 0.0001$) when compared to the control group. Their normalized path length was found to be marginally lower (corrected $p = 0.0930$). No difference in modularity with statistical significance or at trend level was found between the children with hydrocephalus at 12 months post-surgery and the controls. Detailed statistics are included in Table 1.

3.3. Abnormal left hemispheric regional connectivity measures in children with hydrocephalus (Table 2, Table 3, all p values FDR corrected)

In hydrocephalus patients at 3-month post-surgery, 8 regions in the left hemisphere were found to be significantly abnormal in one or more regional connectivity measures. These 8 left hemispheric brain regions included the superior longitudinal gyrus, middle frontal gyrus, middle occipital gyrus, cingulate gyrus, insular, amygdala, caudate, and the thalamus (Table 2). In hydrocephalus patients at 12-month post-surgery, 10 brain regions, including the superior parietal gyrus, superior frontal gyrus, cingulate gyrus, medial frontal gyrus, medial occipital

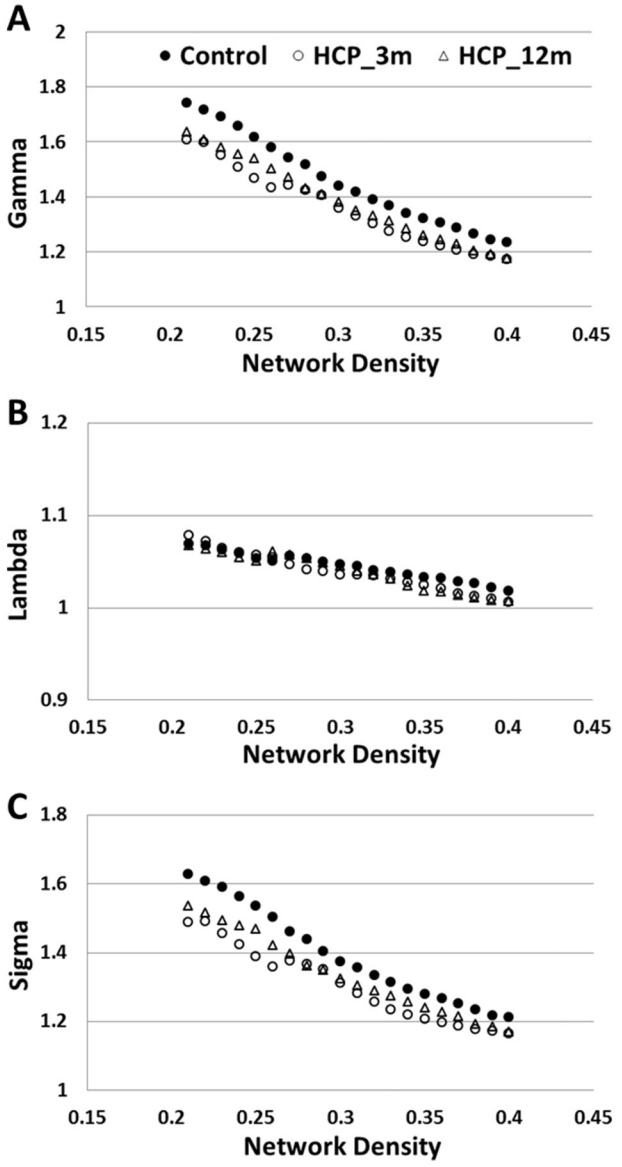

Fig. 3. Characteristics of small-worldness in left hemisphere network in the three study groups. A. Gamma (normalized clustering coefficient); B. lambda (normalized characteristic path length); C. sigma (small-worldness).

gyrus, amygdala, hippocampus, caudate, putamen, and thalamus, were found to be significantly abnormal in one or more of the four regional connectivity measures (Table 3).

3.4. Correlation between left hemispheric structural connectivity measures and contemporaneous developmental outcomes in hydrocephalus patients

Among all the global and regional network measures that had significant group differences, no significant correlation was found with the GAC score tested at the same time as MR imaging.

3.5. Correlation between left hemispheric structural connectivity at 3-month post-surgery and developmental outcomes at 12-months post-surgery

Among the three global network measures that showed significant group differences in hydrocephalus patients at 3-month post-surgery, Eglob tested at 3-month post-surgery was found to be inversely correlated with GAC of the ABAS-II tested at 12 months post-surgery with statistical significance ($r = 0.77$, $n = 9$, corrected $p = 0.045$, Fig. 4). No other global network variables measured at 3 month post-surgery was found to have strong correlation with the GAC score tested at 12 month post-injury.

Among the brain regions with significant group differences in various regional network measures, significant correlations were found between local efficiency in insula and GAC ($r = -0.813$, $n = 9$, corrected $p = 0.029$, Fig. 5A) and between the betweenness centrality in insula and GAC ($r = 0.859$, corrected $p = 0.023$, Fig. 5B).

4. Discussion

One of the challenges in neuroimaging research in children with hydrocephalus post-surgery is the artifact from the programmable shunt valves. In this study we used graph theoretical analysis and DTI tractography to study structural connectivity calculated based only on the left hemisphere network in children with hydrocephalus after surgical treatment. It is expected that the increased intracranial pressure of hydrocephalus would be expressed equally within the cranial cavity. Using unilateral neuroimaging assessment and performing comparisons to controls at different time after surgical treatment can help to alleviate the difficulties resulting from programmable valves. Our main findings are summarized as follows: (1) structural connectivity in the left hemisphere network exhibited small-world attributes in all three study groups (control group, hydrocephalus patients at 3-month post-surgery, hydrocephalus patients at 12-month post-surgery); (2) structural connectivity in the left hemisphere network in children with hydrocephalus differed significantly from the controls at both the global and regional levels in both patient groups; (3) significant correlation was observed between structural connectivity in the left hemisphere in children with hydrocephalus at 3-month post-surgery and the their developmental outcome assessed at 12-month post-surgery.

Table 1
Cross-sectional comparisons of global network measures between HCP patients at 3-month post-injury and the controls and between HCP patients at 12-month post-surgery and the controls. All network values are the area under curve over the network density range between 0.2 and 0.4 (at interval of 0.01) using residual value of network measure based on linear regression to account for age factor at each density level. All *p* values are FDR corrected to minimize false positive findings resulting from multiple comparisons.

Global network measures	CTL $n = 34$	3 m post-surgery HCP $n = 12$				12 m post-surgery HCP $n = 24$			
(AUC of residual value)	Mean ± std	Mean ± std	df	t	*p*	Mean ± std	df	t	*p*
γ	0.0000 ± 0.0321	−0.0392 ± 0.0412	44	−3.38	0.0038*	−0.0243 ± 0.0263	56	−3.06	0.0086*
λ	0.0000 ± 0.0054	−0.0026 ± 0.0060	44	−1.40	ns	−0.0025 ± 0.0047	56	−1.82	0.0930
σ	0.0000 ± 0.0296	−0.0348 ± 0.0338	44	−3.37	0.0026*	−0.0203 ± 0.0229	56	−4.67	0.0113*
E_{glob}	0.0000 ± 0.0037	0.0121 ± 0.0031	44	10.11	<0.0001*	0.0121 ± 0.0030	56	13.11	<0.0001*
MOD	0.0000 ± 0.0076	−0.0048 ± 0.0083	44	−1.83	0.0933	−0.0020 ± 0.0082	56	0.98	NS

Note: AUC = area under curve; γ = normalized clustering coefficient; λ = normalized characteristic path length; σ = small-worldness; E_{glob} = global efficiency; MOD = modularity. ns = not significant. CTL = control; HCP = hydrocephalus.
* *p* value <0.05.

Table 2
HCP patients at 3-month post-surgery, cross-sectional comparisons of regional network measures with the Control Group. Regional network measures include nodal degree, betweenness centrality, clustering coefficient, and nodal efficiency. All regional network values are the area under curve over the network density range between 0.2 and 0.4 (at interval of 0.01) using residual value of network measure based on linear regression to account for age factor at each density level. All p values are FDR corrected across the four network measures and 31 nodes in the network to minimize false positive findings resulting from multiple comparisons. Only those nodes that showed significant group difference in one or more measures are included.

Region	Degree			Betweenness centrality			Clustering coefficient			Local Efficiency		
	CTL n = 34	3 m Post-Surgery n = 12		CTL n = 34	3 m post-surgery n = 12		CTL n = 34	3 m post-surgery n = 12		CTL n = 34	3 m post-surgery n = 12	
	Mean ± std	Mean ± std	t (corrected p)	Mean ± std	Mean ± std	t (corrected p)	Mean ± std	Mean ± std	t (corrected p)	Mean ± std	Mean ± std	t (corrected p)
SPG	0.000 ± 0.825	1.149 ± 1.066	3.84 (0.0069)	0.000 ± 0.016	0.034 ± 0.055	3.29 (0.0222)	0.000 ± 0.024	−0.011 ± 0.030	−1.24 (ns)	0.000 ± 0.015	−0.007 ± 0.022	−1.35 (ns)
CingG	0.000 ± 0.376	1.063 ± 1.050	5.12 (0.0004)	0.000 ± 0.010	0.024 ± 0.032	3.85 (0.0078)	0.000 ± 0.019	0.016 ± 0.034	2.00 (ns)	0.000 ± 0.016	0.012 ± 0.023	1.88 (ns)
MFG	0.000 ± 0.771	−1.117 ± 0.985	−4.01 (0.0057)	0.000 ± 0.009	−0.008 ± 0.011	−2.39 (ns)	0.000 ± 0.038	0.024 ± 0.044	1.81 (ns)	0.000 ± 0.020	0.010 ± 0.019	1.49 (ns)
MOG	0.000 ± 0.675	−1.171 ± 1.543	−3.60 (0.0099)	0.000 ± 0.022	−0.030 ± 0.020	−4.13 (0.0049)	0.000 ± 0.022	0.078 ± 0.120	3.67 (0.0089)	0.000 ± 0.014	0.009 ± 0.063	0.78 (ns)
Ins	0.000 ± 0.474	0.472 ± 0.774	2.50 (ns)	0.000 ± 0.005	0.009 ± 0.012	3.70 (0.0092)	0.000 ± 0.024	−0.020 ± 0.027	−2.44 (ns)	0.000 ± 0.013	−0.011 ± 0.014	−2.59 (0.095)
Amyg	0.000 ± 0.484	0.278 ± 0.567	1.64 (ns)	0.000 ± 0.004	−0.001 ± 0.002	−0.84 (ns)	0.000 ± 0.075	0.102 ± 0.133	3.27 (0.0214)	0.000 ± 0.085	0.103 ± 0.124	3.19 (0.025)
Caud	0.000 ± 0.627	0.660 ± 1.756	1.90 (ns)	0.000 ± 0.004	0.006 ± 0.010	2.91 (0.04978)	0.000 ± 0.082	−0.060 ± 0.121	−1.92 (ns)	0.000 ± 0.080	−0.052 ± 0.124	−1.65 (ns)
Thal	0.000 ± 0.758	−2.007 ± 1.095	−6.99 (<0.0001)	0.000 ± 0.023	−0.036 ± 0.019	−4.81 (0.0007)	0.000 ± 0.024	0.018 ± 0.090	1.08 (ns)	0.000 ± 0.027	−0.019 ± 0.088	−1.15 (ns)

4.1. The inclusion of post-surgical hydrocephalus patients with shunt artifact

In a recent study of whole brain structural connectivity in children with hydrocephalus from our group (Yuan et al., 2015), data from 7 hydrocephalus patients at 3-month post-surgery and 10 hydrocephalus patients at 12-month post-surgery were combined into a single post-surgery patient group. In that study, many patients were excluded from the analysis due to the shunt artifact. In the present study, patients were selected from the same study group. By studying the left hemisphere only, all those patients with right hemisphere programmable shunts became eligible to be included in the analysis. Only one child in the entire patient group was shunted in the left hemisphere and thus was not included in the present study. The larger sample size made it feasible to study the patients at two post-surgery time points separately. It also made it feasible to study the association between structural connectivity and developmental outcome.

Table 3
HCP patients at 12-month post-surgery, cross-sectional comparisons of regional network measures with the Control Group. Regional network measures include nodal degree, betweenness centrality, clustering coefficient, and nodal efficiency. All regional network values are the area under curve over the network density range between 0.2 and 0.4 (at interval of 0.01) using residual value of network measure based on linear regression to account for age factor at each density level. All *p* values are FDR corrected across the four network measures and 31 nodes in the network to minimize false positive findings resulting from multiple comparisons. Only those nodes that showed significant group difference in one or more measures are included.

Region	Degree			Betweenness centrality			Clustering coefficient			Local efficiency		
	CTL *n* = 34	12 m post-surgery n = 24		CTL n = 34	12 m post-surgery n = 24		CTL n = 34	12 m post-surgery n = 24		CTL n = 34	12 m post-surgery n = 24	
	Mean ± std	Mean ± std	t (corrected p)	Mean ± std	Mean ± std	t (corrected p)	Mean ± std	Mean ± std	t (corrected p)	Mean ± std	Mean ± std	t (corrected p)
SPG	0.000 ± 0.825	0.632 ± 1.143	2.45 (0.0772)	0.000 ± 0.016	0.022 ± 0.039	3.00 (0.0313)	0.000 ± 0.024	0.001 ± 0.036	0.11 (ns)	0.000 ± 0.015	−0.001 ± 0.023	−0.16 (ns)
CingG	0.000 ± 0.376	0.961 ± 0.906	5.56 (<0.0001)	0.000 ± 0.010	0.021 ± 0.023	4.79 (0.0004)	0.000 ± 0.019	0.009 ± 0.022	1.69 (ns)	0.000 ± 0.016	0.009 ± 0.016	2.17 (ns)
SFG	0.000 ± 0.927	−0.902 ± 0.854	−3.77 (0.0049)	0.000 ± 0.029	−0.017 ± 0.027	−2.34 (0.0946)	0.000 ± 0.015	0.023 ± 0.033	3.58 (0.0081)	0.000 ± 0.010	0.013 ± 0.022	2.94 (0.031)
MFG	0.000 ± 0.771	−0.688 ± 1.008	−2.95 (0.0323)	0.000 ± 0.009	−0.002 ± 0.012	−0.76 (ns)	0.000 ± 0.038	0.016 ± 0.041	1.56 (ns)	0.000 ± 0.020	0.006 ± 0.024	0.99 (ns)
MOG	0.000 ± 0.675	−0.665 ± 1.109	−2.84 (0.0358)	0.000 ± 0.022	−0.019 ± 0.024	−3.10 (0.0265)	0.000 ± 0.022	0.031 ± 0.034	4.21 (0.0023)	0.000 ± 0.014	0.018 ± 0.020	4.01 (0.004)
Amyg	0.000 ± 0.484	0.526 ± 0.540	3.89 (0.0037)	0.000 ± 0.004	0.002 ± 0.007	1.40 (ns)	0.000 ± 0.075	0.091 ± 0.103	3.90 (0.0040)	0.000 ± 0.085	0.098 ± 0.105	3.91 (0.004)
Hippo	0.000 ± 0.458	0.494 ± 0.849	2.86 (0.0351)	0.000 ± 0.014	0.005 ± 0.015	1.28 (ns)	0.000 ± 0.041	−0.005 ± 0.055	−0.41 (ns)	0.000 ± 0.040	−0.006 ± 0.047	−0.52 (ns)
Caud	0.000 ± 0.627	0.908 ± 1.581	3.04 (0.0300)	0.000 ± 0.004	0.010 ± 0.020	2.89 (0.0341)	0.000 ± 0.082	−0.073 ± 0.076	−3.44 (0.0115)	0.000 ± 0.080	−0.055 ± 0.086	−2.47 (0.076)
Put	0.000 ± 0.613	0.051 ± 1.089	0.23 (ns)	0.000 ± 0.008	0.010 ± 0.016	3.18 (0.0231)	0.000 ± 0.034	−0.030 ± 0.059	−2.42 (0.0802)	0.000 ± 0.033	−0.032 ± 0.063	−2.52 (0.070)
Thal	0.000 ± 0.758	−1.741 ± 1.408	−6.08 (<0.0001)	0.000 ± 0.023	−0.033 ± 0.024	−5.21 (0.0001)	0.000 ± 0.024	0.023 ± 0.043	2.62 (0.0609)	0.000 ± 0.027	−0.007 ± 0.045	−0.73 (ns)

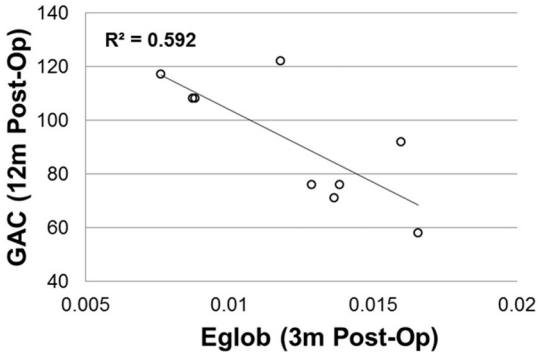

Fig. 4. Correlation between global efficiency at 3-months post-surgery and developmental outcome measure (ABAS-II GAC) tested at 12 m post-surgery.

4.2. Small-worldness attributes in the left hemisphere network

The human brain network has been found to possess the small-worldness feature both functionally (Achard et al., 2006; Wu et al., 2013) and structurally (Van den Heuvel et al., 2010; Hagmann et al., 2010; Dennis et al., 2013) as demonstrated using graph theoretical analysis combined with fMRI and DTI tractography, respectively. This small-worldness feature is a reflection of the balance in network topology between network segregation and integration, which, in terms of structural connectivity, is determined by how tightly the brain regions are connected with other regions in the neighborhood and the amount of long distance connections within the network. In the present study, the connectivity matrix representing the brain network was constructed using the 31 brain regions in the left hemisphere only. Our observation of small-worldness attributes derived from the left hemisphere in the three study groups are consistent with the previous findings about single hemisphere network topology as reported in the literature (Hagmann et al., 2010; Dennis et al., 2013; Li et al., 2014; Caeyenberghs and Leeman, 2014) and supports the notion that small-world topology is a fundamental principle of brain organization (Tian et al., 2011), both for the whole brain network and the left hemisphere network only.

4.3. The abnormalities in left hemisphere structural connectivity

Despite the common small-world topology, in the present study, significant differences in both global and regional network measures were observed in children with hydrocephalus after surgical treatment. Among the global network measures examined in the present study, the left hemisphere small-worldness (σ) in hydrocephalus patients at 3-month post-surgery was significantly lower than the control group driven mainly by the lower normalized clustering coefficient. In hydrocephalus patients at 12-month post-surgery, the normalized clustering coefficient was also significantly lower than the controls. In addition, the normalized characteristic path length in the patient group at 12-month post-surgery had a trend level difference (lower) when compared to the controls. Overall, similar to the patient group at 3-month post-surgery, the small-worldness in patients at 12-month post-surgery remained significantly lower than the controls despite the moderate change in normalized characteristic path length. The findings in the present study are generally consistent with the small-worldness-related global network changes reported in our recent work based on whole brain structural connectivity analysis (Yuan et al., 2015). It was found that the whole brain structural connectivity had a significantly lower normalized clustering coefficient, a significantly lower normalized characteristic path length, and a significantly lower small-worldness in a group of patients with mixed post-surgery time (either 3-month or 12-month post-surgery, Yuan et al., 2015). It is unclear whether the change in the normalized path length is a progressive procedure within the first year of surgery due to the small number of patients with longitudinal imaging data (only 6 overlap between the two patient groups that had both 3-month and 12-month post-surgery imaging data). However, combined with the findings in the present study that showed significantly higher global efficiency, which is an indication of increased level of system integration, the characteristics in the abnormalities observed in the global network measures in the post-surgery hydrocephalus patients suggested disturbance in both the integration (higher global efficiency, lower normalized characteristic path length) and segregation (lower normalized clustering coefficient) aspects of brain network, pointing in the direction of a random network at both 3-month and 12-month post-surgery. Although counter-intuitive (higher global efficiency), this network randomization has been reported in some other disease populations such as patients with schizophrenia, autism, alcoholism, and mild cognitive impairment (Rudie et al., 2012; Alexander-Bloch et al., 2013; Zhou and Lui, 2013; Cao et al., 2014). It has been interpreted as a compensatory mechanism, i.e., the shorter path length (and the complementary higher global efficiency) is an alternative approach in the rewiring of the network when the local efficiency has been compromised (Zhou and Lui, 2013). The "over-pruning" theory has been suggested by Alexander-Bloch et al. (2013) to explain these changes. However, considering the diverse pathological mechanisms in these different neurological diseases, it would be premature to suggest that the brain network in post-surgical hydrocephalus patients has similar patterns of structural plasticity during the course of recovery. Further experimental neuroimaging studies combined with immunohistochemistry are warranted to help elucidate the underlying pathological mechanisms.

In the current study, regional network measures also showed statistically significant group differences for both patient groups when compared to the controls. Specifically, we found 8 regions in the left hemisphere with significant abnormalities in the regional network measures in patients with hydrocephalus at 3-month post-surgery

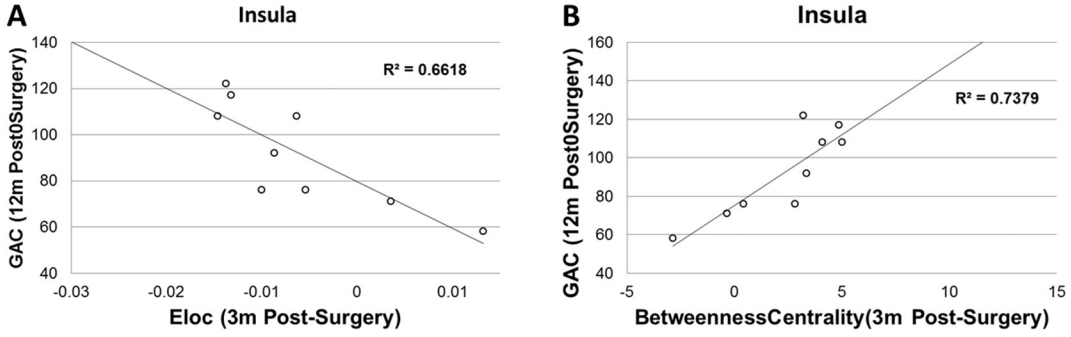

Fig. 5. Correlation between regional network measures at 3 months post-surgery and developmental outcome measures at 12 m post-surgery. A. Eloc in Insular vs. ABAS-II GAC; B. betweenness centrality in insular vs. GAC.

(Table 2). These regions included 4 cortical regions (superior parietal gyrus, cingulate gyrus, medial frontal gyrus, medial occipital gyrus) and 4 subcortical regions (thalamus, insular, amygdala, caudate nucleus). In patients at 12-month post-surgery (Table 3), 5 cortical regions (superior parietal gyrus, cingulate gyrus, medial frontal gyrus, medial occipital gyrus, and superior frontal gyrus) and 5 subcortical regions (thalamus, amygdala, caudate nucleus, putamen, hippocampus) were found to have significant abnormalities in regional network measures. The significant regions from the two study groups are similar. These regions are known to be associated with many essential domains of motor and cognitive functions such as spatial orientation, processing, and navigation, motor control and sensorimotor relay, learning, memory, and executive functions (Dupont et al., 1994; Shulman et al., 1998; Briggs and Usrey, 2008; Waberski et al., 2008; Tanaka et al., 2009; Renier et al., 2010; Schurz et al., 2013; Tu et al., 2013; Lester and Dassonville, 2014). However, it is difficult to identify a consistent pattern in terms of the direction of changes in the regional variables in either cortical or subcortical regions, which may be a reflection of the complex nature of the region-specific changes in WM remained after the treatment.

4.4. Correlation between network measures and contemporaneous developmental outcome

Predicting long-term functional outcome of hydrocephalus patients after surgical treatment has been difficult to ascertain. The present study explored the predictive value of left hemisphere structural connectivity assessed at three month post-surgery for future cognitive outcome measures. We found that the global efficiency as well as the local efficiency and the between-ness centrality in insular cortex in patients at three month post-surgery were significantly correlated with the neuropsychological outcome assessed at 12 month post-surgery. More specifically, children with hydrocephalus at 3-month post-surgery showed lower global efficiency and lower local efficiency and higher betweenness centrality in the insular cortex showed better results in GAC scores tested at 12 months post-surgery. This relation seems to be specific to the post-surgical hydrocephalus patients because correlation analysis in the control group did not show similar association between the structural connectivity and future outcomes.

The insula is an important cortical hub that is involved in a number of crucial functions including cognition, perception, emotion, motor control, somatosensory function, affective domain in learning, and interpersonal skills. Although we did not perform further analysis of the three adaptive domains comprising the GAC (Conceptual, Social, and Practical) that constitute the GAC score due to the lack of statistical power, some skills tested in these domains, e.g., social skills and communication skills, are known to be affected by the integrity of the insular cortex (Levens and Phelps, 2010; Baier et al., 2014; Ruiz et al., 2013; Gasquoine, 2014; Oh et al., 2014; Biduła and Króliczak, 2015). In network connectivity analysis, the insula has also been found to be an important network "hub" in graph theoretical analysis (Power et al., 2013). In addition, previous graph analysis (Harriger et al., 2012) found that the insula was a part of the "rich club" (those highly connected nodes that are also connected to each other) and carried relatively more weight in its contribution to long distance connection at the global level, and thus its change could potentially have a significant impact on the global efficiency as seen in the present study.

4.5. Limitations of the study

A potential limitation in our study is the sample size in both patient groups. Although the approach of using left-hemisphere only has made it practical to study structural connectivity in children with shunt artifacts, we had to exclude almost all infants with hydrocephalus because the signal to noise ratio and pattern of contrast in children at this age range made it difficult to consistently obtain accurate registration results across all the infants. Therefore, the findings from the present study should be considered preliminary and need to be validated in a larger scale study before they can be generalized for the entire patient population. A further issue is the lack of longitudinal data which prevented us from studying the course of recovery in white matter structure connectivity as well as their association with neuropsychological outcomes. In addition, it should be noted that the new findings in the present study were derived from the left hemisphere network only. We cannot rule out the possibility that the right hemisphere may undergo a different course of change and may affect the neuropsychological and behavioral outcomes in a way that is not reflected in the findings based on the left hemisphere. This could be addressed by evaluating patients with left side shunt valves and analyzing their right hemisphere networks. However, this patient population is rare and the limitation is beyond the scope of the current work and should remain for further investigation in future studies.

5. Conclusion

Our data showed that the left hemisphere structural connectivity analysis based on DTI and graph theory was sensitive in detecting both global and regional network abnormality. We showed that the left brain network in children with hydrocephalus retained small-worldness but presented signs of randomized network features within the first year following surgery. In addition, we also demonstrated the ability of our approach to predict future neuropsychological outcomes. The structural connectivity analysis used in the current study is a useful approach with clinical significance that would improve the long-term post-surgical prognosis and potentially allow for early intervention targeted on specific domains of deficits in this common pediatric neurosurgical patient population.

Acknowledgements

This work was supported by the National Institute of Neurological Disorders and Stroke at the National Institutes of Health (R01 NS066932 to W. Y. and F. T. M. and K23 NS075151 to D. D. L), the National Institute of Child Health and Human Development at the National Institutes of Health (P30 HD062171 to J. C.), and the Children's Surgical Sciences Institute at St. Louis Children's Hospital (foundation grant to D. D. L.). J. S. S. was supported by the Intellectual and Developmental Disabilities Research Center at Washington University with funding from the National Institute of Child Health and Human Development (P30 HD062171). Research reported in this publication was also supported in part by the Eunice Kennedy Shriver National Institute of Child Health & Human Development of the National Institutes of Health under Award Number U54 HD087011 to the Intellectual and Developmental Disabilities Research Center at Washington University.

References

Achard, S., Salvador, R., Whitcher, B., Suckling, J., Bullmore, E., 2006. A resilient, low frequency, small-world human brain functional network with highly connected association cortical hubs. J. Neurosci. 26, 63–72.

Air, E.L., Yuan, W., Holland, S.K., Jones, B.V., Bierbrauer, K., Altaye, M., Mangano, F.T., 2010. Longitudinal comparison of pre- and postoperative diffusion tensor imaging parameters in young children with hydrocephalus. J. Neurosurg. Pediatr. 5, 385–391.

Akbari, S.H., Limbrick Jr., D.D., McKinstry, R.C., Altaye, M., Ragan, D.K., Yuan, W., Mangano, F.T., Holland, S.K., Shimony, J.S., 2015. Periventricular hyperintensity in children with hydrocephalus. Pediatr. Radiol. 45, 1189–1197.

Alexander-Bloch, A.F., Vértes, P.E., Stidd, R., Lalonde, F., Clasen, L., Rapoport, J., Giedd, J., Bullmore, E.T., Gogtay, N., 2013. The anatomical distance of functional connections predicts brain network topology in health and schizophrenia. Cereb. Cortex 23, 127–138.

Assaf, Y., Ben-Sira, L., Constantini, S., Chang, L.C., Beni-Adani, L., 2006. Diffusion tensor imaging in hydrocephalus: initial experience. AJNR Am. J. Neuroradiol. 27, 1717–1724.

Baier, B., Eulenburg, P., Geber, C., Rohde, F., Rolke, R., Maihöfner, C., Birklein, F., Dieterich, M., 2014. Insula and sensory insular cortex and somatosensory control in patients with insular stroke. Eur. J. Pain 18, 1385–1393.

Basser, P.J., Pierpaoli, C., 1998. A simplified method to measure the diffusion tensor from seven MR images. Magn. Reson. Med. 39, 928–934.

Ben-Sira, L., Goder, N., Bassan, H., Lifshits, S., Assaf, Y., Constantini, S., 2015. Clinical benefits of diffusion tensor imaging in hydrocephalus. J. Neurosurg. Pediatr. 16, 195–202.
Biduła, S.P., Króliczak, G., 2015. Structural asymmetry of the insula is linked to the lateralization of gesture and language. Eur. J. Neurosci. 41, 1438–1447.
Briggs, F., Usrey, W.M., 2008. Emerging views of corticothalamic function. Curr. Opin. Neurobiol. 18, 403–407.
Buckley, R.T., Yuan, W., Mangano, F.T., Phillips, J.M., Powell, S., McKinstry, R.C., Rajagopal, A., Jones, B.V., Holland, S.K., Limbrick, D.D., 2012. Longitudinal comparison of diffusion tensor imaging parameters and neuropsychological measures following endoscopic third ventriculostomy for hydrocephalus. J. Neurosurg. Pediatr. 9, 630–635.
Caeyenberghs, K., Leemans, A., 2014. Hemispheric lateralization of topological organization in structural brain networks. Hum. Brain Mapp. 35, 4944–4957.
Caeyenberghs, K., Leemans, A., De Decker, C., Heitger, M., Drijkoningen, D., Linden, C.V., Sunaert, S., Swinnen, S.P., 2012. Brain connectivity and postural control in young traumatic brain injury patients: a diffusion MRI based network analysis. Neuroimage Clin. 1, 106–115.
Cao, R., Wu, Z., Li, H., Xiang, J., Chen, J., 2014. Disturbed connectivity of EEG functional networks in alcoholism: a graph-theoretic analysis. Biomed. Mater. Eng. 24, 2927–2936.
Dennis, E.L., Jahanshad, N., McMahon, K.L., de Zubicaray, G.I., Martin, N.G., Hickie, I.B., Toga, A.W., Wright, M.J., Thompson, P.M., 2013. Development of brain structural connectivity between ages 12 and 30: a 4-tesla diffusion imaging study in 439 adolescents and adults. NeuroImage 64, 671–684.
Ding, J.R., An, D., Liao, W., Li, J., Wu, G.R., Xu, Q., Long, Z., Gong, Q., Zhou, D., Sporns, O., Chen, H., 2013. Altered functional and structural connectivity networks in psychogenic non-epileptic seizures. PLoS One 8, e63850.
Djamanakova, A., Faria, A.V., Hsu, J., Ceritoglu, C., Oishi, K., Miller, M.I., Hillis, A.E., Mori, S., 2013. Diffeomorphic brain mapping based on T1-weighted images: improvement of registration accuracy by multichannel mapping. J. Magn. Reson. Imaging 37, 76–84.
Dupont, P., Orban, G.A., De Bruyn, B., Verbruggen, A., Mortelmans, L., 1994. Many areas in the human brain respond to visual motion. J. Neurophysiol. 72, 1420–1424.
Gasquoine, P.G., 2014. Contributions of the insula to cognition and emotion. Neuropsychol. Rev. 24, 77–87.
Hagmann, P., Sporns, O., Madan, N., Cammoun, L., Pienaar, R., Wedeen, V.J., Meuli, R., Thiran, J.P., Grant, P.E., 2010. White matter maturation reshapes structural connectivity in the late developing human brain. Proc. Natl. Acad. Sci. U. S. A. 107, 19067–19072.
Harriger, L., van den Heuvel, M.P., Sporns, O., 2012. Rich club organization of macaque cerebral cortex and its role in network communication. PLoS One 7, e46497.
Harrison, P.L., Oakland, T., 2003. Adaptive Behavior Assessment System. Second edition. The Psychological Corporation, San Antonio, TX.
Hasan, K.M., Eluvathingal, T.J., Kramer, L.A., Ewing-Cobbs, L., Dennis, M., Fletcher, J.M., 2008. White matter microstructural abnormalities in children with spina bifida myelomeningocele and hydrocephalus: a diffusion tensor tractography study of the association pathways. J. Magn. Reson. Imaging 27, 700–709.
He, Y., Dagher, A., Chen, Z., Charil, A., Zijdenbos, A., Worsley, K., Evans, A., 2009. Impaired small-world efficiency in structural cortical networks in multiple sclerosis associated with white matter lesion load. Brain 132, 3366–3379.
Hirsch, J.F., 1992. Surgery of hydrocephalus: past, present and future. Acta Neurochir. 116, 155–160.
Humphries, M.D., Gurney, K., Prescott, T.J., 2006. The brainstem reticular formation is a small-world, not scale-free, network. Proc. Biol. Sci. 273, 503–511.
Jang, S.H., Choi, B.Y., Chang, C.H., Jung, Y.J., Byun, W.M., Kim, S.H., Yeo, S.S., 2013. The effects of hydrocephalus on the periventricular white matter in intracerebral hemorrhage: a diffuser tensor imaging study. Int. J. Neurosci. 123, 420–424.
Jiang, H., van Zijl, P.C., Kim, J., Pearlson, G.D., Mori, S., 2006. DtiStudio: resource program for diffusion tensor computation and fiber bundle tracking. Comput. Methods Prog. Biomed. 81, 106–116.
Kulkarni, A.V., Donnelly, R., Mabbott, D.J., Widjaja, E., 2015. Relationship between ventricular size, white matter injury, and neurocognition in children with stable, treated hydrocephalus. J. Neurosurg. Pediatr. 16, 267–274.
Leemans, A., Jones, D.K., 2009. The B-matrix must be rotated when correcting for subject motion in DTI data. Magn. Reson. Med. 61, 1336–1349.
Lester, B.D., Dassonville, P., 2014. The role of the right superior parietal lobule in processing visual context for the establishment of the egocentric reference frame. J. Cogn. Neurosci. 26, 2201–2209.
Levens, S.M., Phelps, E.A., 2010. Insula and orbital frontal cortex activity underlying emotion interference resolution in working memory. J. Cogn. Neurosci. 22, 2790–2803.
Li, M., Chen, H., Wang, J., Liu, F., Long, Z., Wang, Y., Iturria-Medina, Y., Zhang, J., Yu, C., Chen, H., 2014. Handedness- and hemisphere-related differences in small-world brain networks: a diffusion tensor imaging tractography study. Brain Connect. 4, 145–156.
Liu, M., Chen, Z., Beaulieu, C., Gross, D.W., 2014. Disrupted anatomic white matter network in left mesial temporal lobe epilepsy. Epilepsia 55, 674–682.
Mangano, F.T., Altaye, M., McKinstry, R.C., Shimony, J.S., Powell, S.K., Phillips, J.M., Barnard, H., Limbrick Jr., D.D., Holland, S.K., Jones, B.V., Dodd, J., Simpson, S., Mercer, D., Rajagopal, A., Bidwell, S., Yuan, W., 2016. DTI study of children with congenital hydrocephalus: 1 year post-surgical outcomes. J. Neurosurg. Pediatr. 2016 (May 20), 1–14 (Epub ahead of print).
Mataro, M., Junque, C., Poca, M.A., Sahuquillo, J., 2001. Neuropsychological findings in congenital and acquired childhood hydrocephalus. Neuropsychol. Rev. 11, 169–178.
Oh, A., Duerden, E.G., Pang, E.W., 2014. The role of the insula in speech and language processing. Brain Lang. 135, 96–103.
Oishi, K., Zilles, K., Amunts, K., 2008. Human brain white matter atlas: identification and assignment of common anatomical structures in superficial white matter. NeuroImage 43, 447–457.
Oishi, K., Faria, A., Jiang, H., Li, X., Akhter, K., Zhang, J., Hsu, J.T., Miller, M.I., van Zijl, P.C., Albert, M., Lyketsos, C.G., Woods, R., Toga, A.W., Pike, G.B., Rosa-Neto, P., Evans, A., Mazziotta, J., Mori, S., 2009. Atlas-based whole brain white matter analysis using large deformation diffeomorphic metric mapping: application to normal elderly and Alzheimer's disease participants. NeuroImage 46, 486–499.
Pereira, J.B., Aarsland, D., Ginestet, C.E., Lebedev, A.V., Wahlund, L.O., Simmons, A., Volpe, G., Westman, E., 2015. Aberrant cerebral network topology and mild cognitive impairment in early Parkinson's disease. Hum. Brain Mapp. 36, 2980–2995.
Power, J.D., Schlaggar, B.L., Lessov-Schlaggar, C.N., Petersen, S.E., 2013. Evidence for hubs in human functional brain networks. Neuron 79, 798–813.
Ragan, D.K., Cerqua, J., Nash, T., McKinstry, R.C., Shimony, J.S., Jones, B.V., Mangano, F.T., Holland, S.K., Yuan, W., Limbrick Jr., D.D., 2015. The accuracy of linear indices of ventricular volume in pediatric hydrocephalus: technical note. J. Neurosurg. Pediatr. 15, 547–551.
Rajagopal, A., Shimony, J.S., McKinstry, R.C., Altaye, M., Maloney, T., Mangano, F.T., Limbrick, D.D., Holland, S.K., Jones, B.V., Simpson, S., Mercer, D., Yuan, W., 2013. White matter microstructural abnormality in children with hydrocephalus detected by probabilistic diffusion tractography. Am. J. Neuroradiol. 34, 2379–2385.
Renier, L.A., Anurova, I., De Volder, A.G., Carlson, S., Van Meter, J., Rauschecker, J.P., 2010. Preserved functional specialization for spatial processing in the middle occipital gyrus of the early blind. Neuron 68, 138–148.
Rubinov, M., Sporns, O., 2010. Complex network measures of brain connectivity: uses and interpretations. NeuroImage 52, 1059–1069.
Rudie, J.D., Brown, J.A., Beck-Pancer, D., Hernandez, L.M., Dennis, E.L., Thompson, P.M., Bookheimer, S.Y., Dapretto, M., 2012. Altered functional and structural brain network organization in autism. Neuroimage Clin. 2, 79–94.
Ruiz, S., Lee, S., Soekadar, S.R., Caria, A., Veit, R., Kircher, T., Birbaumer, N., Sitaram, R., 2013. Acquired self-control of insula cortex modulates emotion recognition and brain network connectivity in schizophrenia. Hum. Brain Mapp. 34, 200–212.
Scheel, M., Diekhoff, T., Sprung, C., Hoffmann, K.T., 2012. Diffusion tensor imaging in hydrocephalus—findings before and after shunt surgery. Acta Neurochir. 154, 1699–1706.
Schurz, M., Aichhorn, M., Martin, A., Perner, J., 2013. Common brain areas engaged in false belief reasoning and visual perspective taking: a meta-analysis of functional brain imaging studies. Front. Hum. Neurosci. 7, 712.
Shulman, G.L., Schwarz, J., Miezin, F.M., Petersen, S.E., 1998. Effect of motion contrast on human cortical responses to moving stimuli. J. Neurophysiol. 79, 2794–2803.
Sun, Y., Chen, Y., Lee, R., Bezerianos, A., Collinson, S.L., Sim, K., 2016. Disruption of brain anatomical networks in schizophrenia: a longitudinal, diffusion tensor imaging based study. Schizophr. Res. 171, 149–157.
Tanaka, E., Inui, K., Kida, T., Kakigi, R., 2009. Common cortical responses evoked by appearance, disappearance and change of the human face. BMC Neurosci. 10, 38.
Tian, L., Wang, J., Yan, C., He, Y., 2011. Hemisphere- and gender-related differences in small-world brain networks: a resting-state functional MRI study. NeuroImage 54, 191–202.
Tu, S., Qiu, J., Martens, U., Zhang, Q., 2013. Category-selective attention modulates unconscious processes in the middle occipital gyrus. Conscious. Cogn. 22, 479–485.
Van den Heuvel, M.P., Mandl, R.C.W., Stam, C.J., Kahn, R.S., Hulshoff, P.H.E., 2010. Aberrant frontal and temporal complex network structure in schizophrenia: a graph theoretical analysis. J. Neurosci. 30, 15915–15926.
Waberski, T.D., Gobbelé, R., Lamberty, K., Buchner, H., Marshall, J.C., Fink, G.R., 2008. Timing of visuo-spatial information processing: electrical source imaging related to line bisection judgements. Neuropsychologia 46, 1201–1210.
Wang, R., Benner, T., Sorensen, A.G., Wedeen, V.J., 2007. Diffusion Toolkit: a software package for diffusion imaging data processing and tractography. Proc. Int. Soc. Magn. Reson. Med. 15, 3720.
Watts, D.J., Strogatz, S.H., 1998. Collective dynamics of 'small-world' networks. Nature 393, 440–442.
Wiswell, T.E., Tuttle, D.J., Northam, R.S., Simonds, G.R., 1990. Major congenital neurologic malformations. A 17-year survey. Am. J. Dis. Child. 144, 61–67.
Woods, R.P., Grafton, S.T., Watson, J.D., Sicotte, N.L., Mazziotta, J.C., 1998. Automated image registration: II. Intersubject validation of linear and nonlinear models. J. Comput. Assist. Tomogr. 22, 153–165.
Wu, K., Taki, Y., Sato, K., Hashizume, H., Sassa, Y., Takeuchi, H., Thyreau, B., He, Y., Evans, A.C., Li, X., Kawashima, R., Fukuda, H., 2013. Topological organization of functional brain networks in healthy children: differences in relation to age, sex, and intelligence. PLoS One 8, e55347.
Yuan, W., Mangano, F.T., Air, E.L., Holland, S.K., Jones, B.V., Altaye, M., Mangano, F.T., 2009. Anisotropic diffusion properties in infants with hydrocephalus: a diffusion tensor imaging study. AJNR Am. J. Neuroradiol. 30, 1792–1798.
Yuan, W., Holland, S., Shimony, J., Jones, B.V., Mangano, F.T., Limbrick, D.D., et al., 2011. Quality assurance in multi-institution and multi-scanner MRI Neuroimaging Research. IPR LONDON 2011 6th Congress and Exhibition of the Joint Societies of Paediatric Radiology, London, UK, May 27–31.
Yuan, W., McKinstry, R.C., Shimony, J.S., Altaye, M., Powell, S.K., Phillips, J.M., Limbrick Jr., D.D., Holland, S.K., Jones, B.V., Rajagopal, A., Simpson, S., Mercer, D., Mangano, F.T., 2013. Diffusion tensor imaging properties and neurobehavioral outcomes in children with hydrocephalus. AJNR Am. J. Neuroradiol. 34, 439–445.
Yuan, W., Holland, S.K., Shimony, J.S., Altaye, M., Mangano, F.T., Limbrick, D.D., Jones, B.V., Nash, T., Rajagopal, A., Simpson, S., Ragan, D., McKinstry, R.C., 2015. Abnormal structural connectivity in the brain networks of children with hydrocephalus. Neuroimage Clin. 8, 483–492 (eCollection 2015).
Zhou, Y., Lui, Y.W., 2013. Small-world properties in mild cognitive impairment and early Alzheimer's disease. A Cortical Thickness MRI Study. ISRN Geriatr. (pii: 542080).